Lab on a Chip

Miniaturisation for chemistry, physics, biology, materials science and bioengineering

www.rsc.org/loc

Volume 12 | Number 4 | 21 February 2012 | Pages 665–836

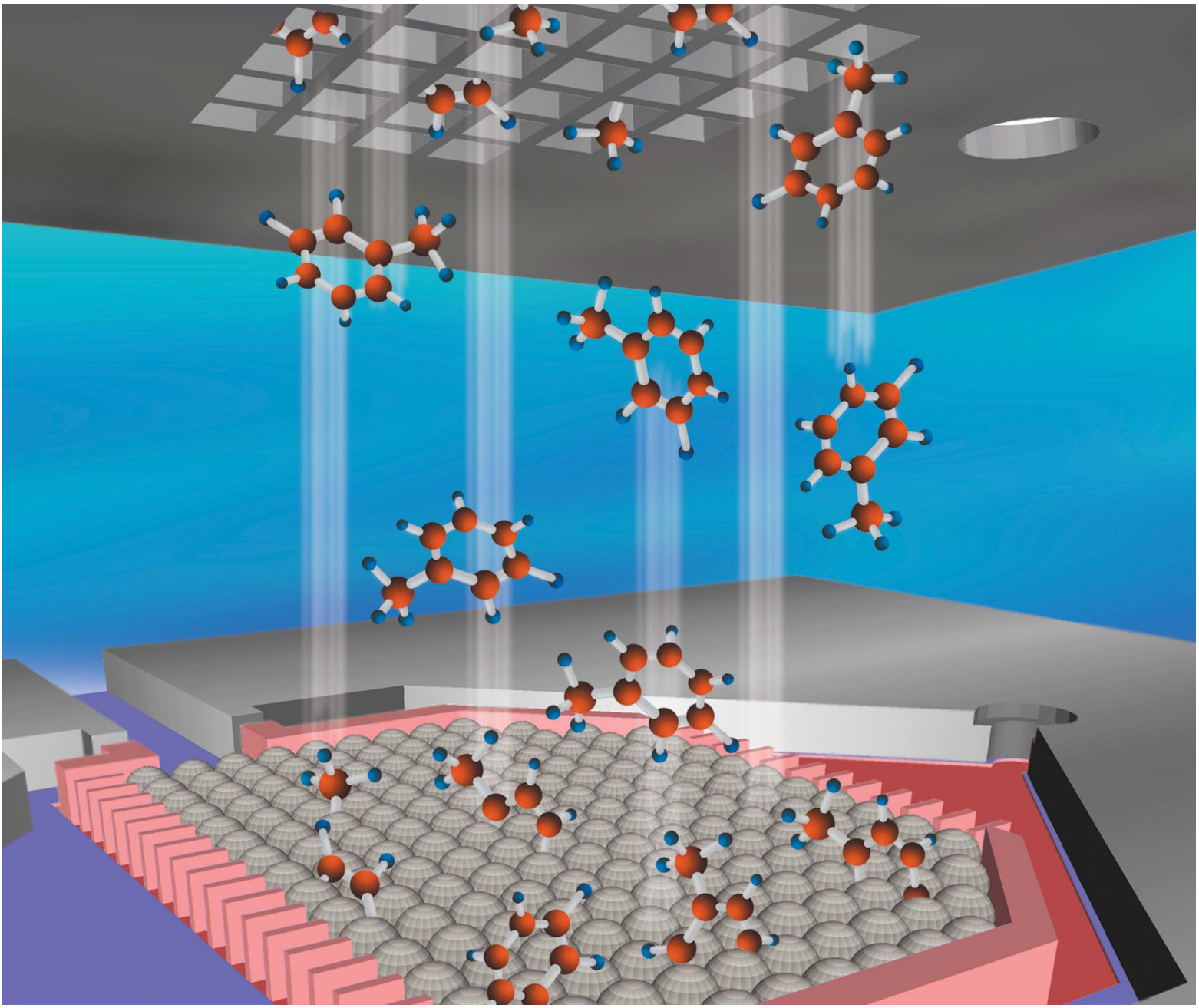

ISSN 1473-0197

RSC Publishing

PAPER

Kurabayashi *et al.*

Microfabricated passive vapor preconcentrator/injector designed for microscale gas chromatography

Lab on a Chip

Dynamic Article Links

Cite this: *Lab Chip*, 2012, **12**, 717

www.rsc.org/loc

PAPER

Microfabricated passive vapor preconcentrator/injector designed for microscale gas chromatography†

Jung Hwan Seo,[ab] Sun Kyu Kim,[ad] Edward T. Zellers*[ade] and Katsuo Kurabayashi*[abc]

Received 27th September 2011, Accepted 5th December 2011
DOI: 10.1039/c2lc20932b

The design, fabrication, and preliminary testing of a micromachined-Si passive vapor preconcentrator/injector (μPPI) are described. Intended for incorporation in a gas chromatographic microsystem (μGC) for analyzing organic vapor mixtures, the μPPI captures vapors from the air at a known rate by means of passive diffusion (*i.e.*, without pumping) and then desorbs the vapor sample thermally by means of an integrated heater and injects it downstream (with pumping). The μPPI chip comprises a 1.8 μL deep reactive-ion-etched (DRIE) Si cavity with a resistively heated membrane floor and a DRIE-Si cap containing >1500 parallel diffusion channels, each 54 × 54 × 200 μm. The cavity is packed with 750 μg of a commercial graphitized carbon adsorbent. Fluidic and heat-transfer modeling was used to guide the design process to ensure power-efficient sample transfer during thermal desorption. Experiments performed with toluene at concentrations of ~1 ppm gave a constant sampling rate of 9.1 mL min^{-1} for up to 30 min, which is within 2% of theoretical predictions and corresponds to a linear dynamic mass uptake range of ~1 μg. The cavity membrane could be heated to 250 °C in 0.23 s with 1 W of applied power and, with 50 mL min^{-1} of suction flow provided by a downstream pump, yielded >95% desorption/injection efficiency of toluene samples over an 8-fold range of captured mass.

Introduction

Gas chromatographic microsystems (μGCs) offer the potential for analyzing mixtures of volatile organic compounds (VOCs) in miniature packages suitable for personal exposure monitoring, point-of-care medical diagnostics, explosive detection, and other applications. Examples of functional prototype μGCs, which we define as comprising, at a minimum, a preconcentrator or a sample injector, separation column, and detector, all of which are microfabricated from Si, glass, or other suitable materials, have appeared in recent years.[1–6]

Often, it is necessary to concentrate the VOC(s) of interest prior to analysis because most detectors lack the inherent sensitivity required to attain the low detection limits demanded in many applications. For this reason, μGC injectors that incorporate a preconcentration function are common. Numerous reports have appeared on microfabricated preconcentrators, which typically consist of a micromachined device with an internal cavity packed or lined with an adsorbent material.[7–15] The VOCs in an air sample, drawn through the device by means of a small pump, are trapped on the surface of the (typically) high-surface-area solid adsorbent. Subsequent rapid heating leads to desorption into a carrier gas flowing at a lower rate, which leads to an enhancement in concentration of the VOCs that are passed downstream to a separation microcolumn and/or a microsensor or microsensor array.

One important factor affecting performance is the dynamic adsorption capacity, which is related to the volatility and functionality of the VOC(s), the mass and specific surface area of the adsorbent (and therefore the size/mass of the device), and the flow rate of the air sample being drawn through the device. Other important performance factors are the desorption rate, efficiency, and bandwidth, which are also related to the volatility and functionality of the VOC(s), the mass and surface area of the adsorbent, and the desorption/injection flow rate, as well as the maximum temperature and rate at which the device is heated. Power requirements also come into play, and often have a significant influence on device design.

As progress is made toward smaller and more power efficient μGC components, the power required for pumping becomes more significant. Although a few reports on low-power,

[a]*Engineering Research Center for Wireless Integrated Microsensing and Systems (WIMS²), University of Michigan, Ann Arbor, MI, 48109, USA*
[b]*Department of Mechanical Engineering, University of Michigan, Ann Arbor, MI, 48109, USA. E-mail: katsuo@umich.edu; Fax: +1-734-647-3170; Tel: +1-734-615-5211*
[c]*Department of Electrical Engineering and Computer Science, University of Michigan, Ann Arbor, MI, 48109, USA*
[d]*Department of Environmental Health Sciences, University of Michigan, Ann Arbor, MI, 48109, USA. E-mail: ezellers@umich.edu; Fax: +1-734-763-8095; Tel: +1-734-936-0766*
[e]*Department of Chemistry, University of Michigan, Ann Arbor, MI, 48109, USA*

† Electronic supplementary information (ESI) available. See DOI: 10.1039/c2lc20932b

microfabricated pumps used in μGC separations have appeared,[5,16] most μGC systems rely on commercial mini-pumps, which dissipate on the order of 1–4 W;[1–6,17–19] this is comparable to the power required for heating state-of-the-art microscale preconcentrators and separation columns.[7,11,12,20,21] Depending on the required sample volume and the time of analysis, the energy for pumping may exceed that for the other power-intensive components.

Passive diffusional samplers were developed nearly 40 years ago for sampling the breathing zone of workers potentially exposed to VOCs,[22] and they are used routinely in environmental and occupational exposure monitoring.[23–27] Most commercial passive VOC samplers are small (*i.e.*, a few cm^3), employ carbon-based trapping materials, and have sampling rates of ~3 to 30 mL min^{-1}. Following the sample collection period, typically 4–24 h, the sampler is returned to the laboratory for solvent or thermal desorption followed by conventional GC analysis. Although a miniaturized passive sampler has been reported,[28,29] there have been no reports on a microfabricated passive sampler with or without an integral heater.

In this article, we report on a microfabricated passive preconcentrator–injector (μPPI) that captures vapors from the air at a known rate by diffusion, without a pump. The μPPI has a top layer with a grid of precisely defined micrometre-scale channels through which VOCs diffuse, and a bottom layer with a thermally isolated, adsorbent packed cavity, tapered inlet/outlet sections with fluidic ports, and an integrated heater on the underside of the cavity floor for desorbing and injecting captured VOCs downstream upon completion of a specified sampling period. The next section provides a brief overview of diffusional sampling theory and the scaling laws relevant to miniaturization. A general description of the μPPI is then presented, followed by the detailed design specifications, the fabrication process, and methods used for testing performance. The power dissipation and response time of the device heating function along with results of initial gravimetric tests of the mass uptake rate using toluene as the test vapor are then briefly summarized. Finally, chamber tests showing the operation of the μPPI are presented, with an emphasis on documenting the sampling rate, capacity, and desorption (injection) capture efficiency of toluene as a function of flow rate.

Background and theory of passive sampling

Passive samplers rely on the diffusion of vapors down a concentration gradient created within the device by placing an adsorbent trap at the end of a stagnant chamber that is open to the ambient. Assuming that the air concentration is effectively zero at the surface of the trap, the diffusional sampling rate is given by the following equation, derived from Fick's first law of diffusion:[30]

$$S = \frac{DA}{L} = \frac{m}{Ct} \quad (1)$$

where D is the diffusion coefficient of the vapor ($cm^2\ s^{-1}$), A is the cross-sectional area of the sampler (cm^2), L is the length of the diffusion path within the sampler (cm), C is the ambient vapor concentration (μg cm^{-3}), and m is the mass of vapor captured (μg) over the sampling time, t (s).

In the absence of turbulence, S is directly proportional to A and inversely proportional to L, and it is theoretically possible to scale down the size of the sampler while keeping S constant by maintaining a constant L/A ratio. In one sequence of articles, Gonzalez and Levine[28,29] described a miniature passive sampler consisting of a cylindrical steel thimble, with a charcoal-pad trap and wire mesh cap. The dimensions of the device, $A = 32\ mm^2$ and $L = 3.8$ mm, resulted in a sampling rate for benzene of 2.8 mL min^{-1}, which is relatively low due to the small A/L ratio of 8.4. This sampling rate could be maintained for 30 min at a challenge concentration of ~0.8 ppm of benzene, after which it started to taper off due to the limited capacity of the adsorbent.

At low vapor concentrations and sub-monolayer coverage of the adsorption sites on the trapping material, the amount of vapor adsorbed to the surface of a granular adsorbent at equilibrium is proportional to the air concentration of the vapor. It can be expressed as the equilibrium adsorption capacity, W_e, which is the ratio of the mass of adsorbed vapor to the mass of adsorbent material.[31] As a monolayer is approached, W_e no longer increases in proportion to the air concentration of the vapor, and at a full monolayer W_e reaches a constant value. In the sub-monolayer regime, the adsorbent serves as an effective vapor trap and the concentration of vapor near the surface can be assumed to be close to zero, so that the sampling rate is governed by eqn (1). As the sites on the adsorbent gradually become occupied, the trapping efficiency is expected to decrease along with the sampling rate. The point at which the sampling rate decreases significantly is a function of time and the vapor concentration, and it defines the effective capacity or service life, as explored below.

Once the sampling period is concluded it is necessary to desorb the captured vapors for analysis. For a microfabricated device, this could be done thermally by heating the adsorbent *in situ* and drawing the released VOCs to downstream components by means of a small pump. This was the approach taken for the μPPI described here. Designing the device for power-efficient heating is therefore important. In addition, sufficient suction flow velocity must be provided to overcome the back-diffusion velocity imparted to the VOCs by the heating process so they do not escape through the inlet aperture. The material properties, fluidic paths, dimensional constraints, heat transfer efficiency, and velocity profiles related to these design and operating variables must all be accounted for in order to realize a viable microscale device suitable for use in the quantitative analysis of VOCs.

General description

Fig. 1 shows a block diagram of a hypothetical microscale GC (μGC) system that incorporates the μPPI as the vapor capture device. A focuser is included because the (pump-driven) flow rate required for delivering desorbed samples from the μPPI to the microcolumn is expected (see below) to exceed the maximum flow rate typically used in μGC separations (*i.e.*, <5 mL min^{-1}). Although splitting the flow downstream from the μPPI could be considered, a properly configured focuser can function as an efficient VOC trap at relatively high flow rates and then be heated rapidly to inject a VOC sample at a (lower) flow rate more compatible with efficient chromatographic separations.[6] The

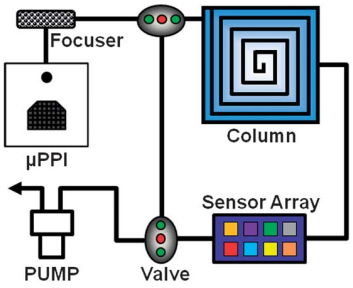

Fig. 1 Conceptual layout diagram of a microscale gas chromatograph (μGC) incorporating the μPPI wherein vapor samples would be collected passively, transferred to a (micro)focuser, injected to the microcolumn for separation, and detected by an array of microsensors.

(entire) injected mixture of VOCs would then be separated in the microcolumn and detected by an array of microsensors.[1,6]

Fig. 2 shows an exploded-view illustration of the μPPI along with side-view illustrations of the sampling and desorption processes, and Fig. 3 provides more detailed diagrams and images of selected device features. The top layer contains a grid of square diffusion channels through which vapors pass into the device (Fig. 3A). This layer also has a through-hole used for fluidic interconnection to downstream components upon thermal desorption/injection of capture VOC samples. The bottom layer contains a cavity with tapered entrance/exit pathways on two sides and a set of walls and pillar structures to retain the adsorbent granules in its central region (Fig. 3B). The area of this central region matches that of the diffusion-channel grid in the top layer. The (desorption) inlet and adsorbent filling ports are located at one end of the cavity, and there are two internal side ports that help to distribute the airflow during thermal desorption. The underside of the membrane floor of the cavity has a meander-line metal thin-film heater and a resistance temperature device (RTD) for thermal desorption (Fig. 3C). The desorbed vapors are drawn through the outlet port and injected onto the downstream focuser.

Device design and expected performance

The top layer Si-substrate thickness, which defines the diffusional path length through the grids, L_1, was set at 200 μm. The aperture of each element in the diffusion-channel grid was set at 54 × 54 μm (grid walls = 12 μm wide). The grid can be viewed as a rectangular subsection with dimensions of 3.2 mm × 1.7 mm and a trapezoidal subsection with dimensions of 3.2 mm

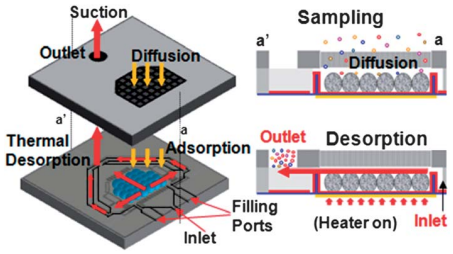

Fig. 2 Exploded view conceptual diagram of μPPI and side views showing the diffusional sampling and thermal desorption processes.

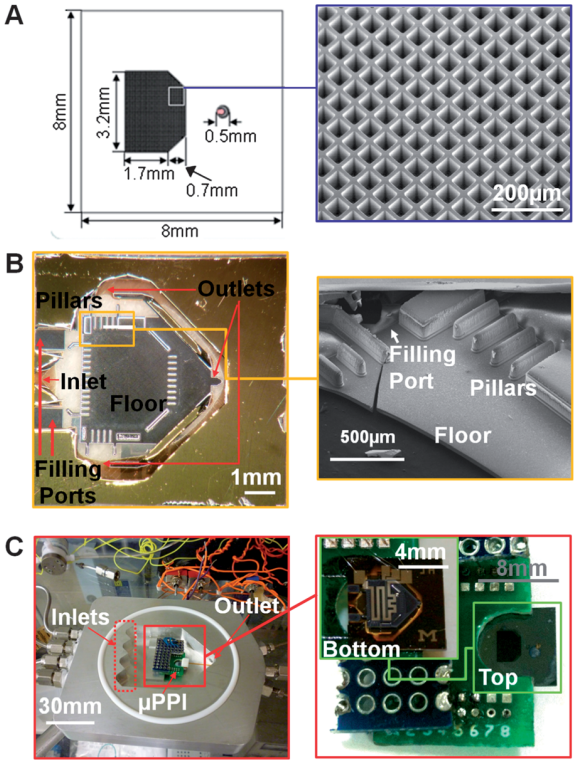

Fig. 3 Images of (A) top layer, (B) bottom layer, and (C) assembled μPPI system in the exposure chamber. The fabricated top layer is shown in (A). After bonding the top and bottom layers, the adsorbent particles are drawn by suction in through the filling ports and retained within the heated area of the cavity by the side walls and pillars (the filling ports would subsequently be sealed). The right-hand image of (B) shows a 3D SEM image of the bottom layer near one of the filling ports. In (C) the packaged μPPI is shown mounted in the exposure chamber.

(long side), 1.8 mm (short side), and 0.7 mm (width), the sum of which contain 1530 channels with an overall area, A_1, of 4.5 mm^2.

Note that the need for a turbulence barrier arises if $L/d < 2.5$, where d is the diameter of the sampling aperture.[32] Below this value of L/d, the path length can be effectively reduced in windy environments by eddy currents created at the entrance to the sampler, to an extent that increases the sampling rate significantly. For an effective grid aperture diameter of 61 μm (derived from a circle having the same area as each grid-aperture square), the value of L_1/d for each channel in the μPPI is 3.3, and the effects of turbulence should be negligible.

The cavity in the bottom layer was designed with a small headspace volume above the adsorbent layer to facilitate adsorbent loading and the subsequent capture of desorbed vapors. Since vapors must diffuse through this gap, it affects the sampling rate. For the selected bottom layer Si-substrate thickness of 250 μm, the cavity floor thickness was limited to 24 μm (*via* boron-doping level, considering mechanical strength, thermal isolation, and heat transfer as discussed below) to give a cavity depth of 226 μm. The adsorbent granules were sieved to a nominal average diameter of 200 μm. Assuming spherical particles, the characteristic length (thickness) for the single-layer adsorbent bed is 161 μm (see Fig. S1 and the associated text in the ESI†). This results in an effective diffusional path length through

the headspace, L_2, of 65 μm. The cross-sectional area of the headspace, A_2, is 6.7 mm^2 (note: A_2 is larger than A_1 because of the lack of any grid walls in the headspace).

Given the serial flow resistance through the grid and then the headspace (note: diffusion into the interstitial spaces between particles is ignored), the effective sampling rate, S_e, can be estimated as follows (see also Fig. S2 and accompanying text in the ESI†):

$$S_e = D\frac{A_1A_2}{A_1L_2 + A_2L_1} \quad (2)$$

Using the values of the variables given above and a value of $D = 0.0849$ cm^2 s^{-1} (25 °C) for toluene,[30] eqn (2) yields an expected sampling rate of 9.3 mL min^{-1} for the μPPI.

The graphitized carbon Carbopack X (C–X) was chosen as the adsorbent material on the basis of previous work indicating that it would have a high affinity for toluene (and other similarly volatile VOCs), which was used as the test vapor, while also allowing efficient thermal desorption.[33,34] This material also has a low affinity for water vapor. The amount of C–X that could be packed into the device was estimated to be about 680 μg on the basis of the cavity volume and the published packing density for 60/80 mesh C–X of 0.41 g cm^{-3},[35] and was subsequently determined gravimetrically to be 750 μg for the sieved C–X used in the actual device. Since the W_e value for toluene at 1 ppm on C–X is 2800 μg g^{-1},[8] the capacity of the device is 2.1 μg of toluene. At 9.3 mL min^{-1}, saturation would be expected after ~60 min of exposure. Since S_e is expected to decline prior to this point, the maximum time between successive thermal desorption/regeneration cycles should be somewhat less than this value.

The primary design factors considered with respect to the desorption of VOCs from the μPPI were the heating rate and power, and the air velocity required to capture (inject) the desorbed vapors. A target maximum desorption temperature of 250–300 °C was chosen on the basis of previous work.[10,33,34] The membrane floor thickness of 24 μm for the cavity represents a compromise between minimizing thermal mass, which promotes rapid, low-power heating, and maximizing mechanical rigidity, which reduces stress-induced deflection and increases the robustness of the overall structure. Although the high thermal conductivity of the p-doped Si (~150 W m^{-1} K^{-1}) promotes the rapid distribution of heat from the underlying heater to the entire adsorbent bed, it demands thermal isolation from the surrounding substrate. Therefore, a 15 μm layer of SiON (thermal conductivity = 5 W m^{-1} K^{-1}) was deposited beneath the cavity floor membrane and the perimeter of the Si membrane was removed so that the cavity floor was suspended on the SiON. A combination of lateral wall structures and arrays of pillars was required at the edges of the Si membrane to retain the adsorbent within the heated region; in the case of the latter there was also a need to allow airflow to pass with minimal flow resistance. A Ti/Pt meander-line heater was then patterned on the underside of the SiON to enable the uniform heating of the cavity and precise, programmable temperature control with low power. Thermal modeling, which accounted for the thermal contact resistance of the adsorbent layer and the convective cooling from the airflow during thermal desorption, indicated that ~1 W of power would raise the membrane temperature to 300 °C in 3 s and that the adsorbent bed temperature would be within the targeted range.

Turning now to the fluidic factors, the first issue considered was the temperature dependence of D, which varies as the square of the temperature ratio, T_2/T_1, where T_1 is the reference temperature and T_2 is the desorption temperature.[30] For toluene, this leads to a D value of 0.31 cm^2 s^{-1} at 300 °C. Assuming the flux out of the device is governed entirely by back diffusion, the expected volumetric flow rate upward during desorption, by eqn (2), is 34 mL min^{-1}, which corresponds to a linear velocity through the headspace of 0.1 m s^{-1}.

The suction flow velocity required by the downstream pump to avoid loss of toluene through the diffusion-channel grid was estimated using CFD analysis (CFD-ACE, ESI Group, Paris, France).[36] The CFD analysis considered the cavity dimensions, the inlet/outlet port locations and the transition geometries, and initially assumed that the entering flow came from the inlet and the grids and the exiting flow went only through the outlet port (*i.e.*, the side ports were not considered).

Simulated flow patterns and trajectories were examined as a function of applied suction pressure, taking into account both the forced convection by the airflow and the back-diffusion of the desorbed vapor. Criteria used to determine performance were the presence of any points where the vertical (z-direction) velocity was positive at an elevation corresponding to the top surface of the grid, and the number and locations of stagnant loci or vortices indicative of low fluid motion within the interior cavity zone. To keep the computational task reasonable, the presence of the adsorbent granules was ignored (note: it can be shown that the empty cavity represents a more conservative constraint in terms of preventing the vapor loss due to the back diffusion (see Fig. S3 and the associated text in the ESI†)).

CFD simulations of numerous possible design variations and flow conditions revealed the importance of using tapered inlet and outlet transitions to promote the uniformity of the flow profile across the width of the cavity, and adding side port exit paths toward the upstream end of the cavity to ensure that the vertical velocity remained negative in this region. A minimum pressure drop of 15 kPa between the inlet and the outlet was required to avoid loss of vapor through the top-layer grid and to eliminate vapor stagnation in the cavity. This pressure drop translates into a minimum flow rate of ~60 mL min^{-1} (1.25 m s^{-1}).

Experimental

Microfabrication and assembly

Wafers of p-doped ⟨100⟩ Si, 200 μm and 250 μm thick, were used to fabricate the top and bottom layers of the μPPI, respectively. The former was double-side polished and the latter was single-side polished. In fabricating the top layer (Fig. S4A†), a Cr/Au (10/450 nm) layer was first evaporated onto the backside and the grid wall pattern was defined with photoresist. Au was then electroplated to a thickness of 3–4 μm on the perimeter of the backside of the top layer for subsequent eutectic bonding. After stripping, a new photoresist layer was patterned to expose the grid apertures and the thin Cr/Au layers were removed by wet etching. Through-wafer deep reactive ion etching (DRIE) was used to create the diffusion grid and the outlet port.

The bottom layer fabrication (Fig. S4B†) started with the growth of a 15 μm thick thermal oxide layer on the backside of

the wafer, which was then patterned to permit formation of the pillars (height: 170–190 μm; width: 90 μm; spacing: 100 μm), the lateral walls (height: 170–190 μm; width: 130–440 μm), the side ports (width: 780 μm), and the side-port flow channels (height: 250 μm; width: 260 μm) by DRIE. After that, the oxide layer was stripped. Then, a 24 μm thick boron-doped Si layer was formed on the backside of the cavity floor by a standard boron diffusion process for ~17 h. A 15 μm thick low-stress SiON layer was then deposited on the backside by plasma-enhanced chemical vapor deposition (PECVD). The Ti/Pt meander-line microheater and the resistive temperature sensor were then patterned and deposited on the oxy-nitride layer by a lift-off process, followed by annealing at 400 °C to relieve thermal stress. A Ti/Au mask layer was then deposited and patterned on the front side of the bottom layer for eutectic bonding and DRIE was used to complete the formation of the cavity-floor membrane, filling ports, inlet, and pillars. Finally, etching in ethylenediamine–pyrocatechol (EDP) removed residual undoped Si.

Top- and bottom-layer structures were diced, aligned, and temporarily fixed to each other using a small amount of epoxy (Durapot 865, Cotronics, NY). This was followed by eutectic bonding of the two layers at 330 °C for 12 hours. The device was fixed to a set of pins on a small section of a printed circuit board (PCB) and the on-chip heater and the RTD on the bottom layer were wire bonded to traces on the PCB. A capillary connector with right-angle circular channels was fashioned from a piece of Macor® and was bonded to the outlet port in the top layer using epoxy (Duraseal 1531, Cotronics, Brooklyn, NY), and then a section of a deactivated fused-silica capillary (i.d.: 530 μm) was inserted and sealed with the same epoxy.

A sample of 60/80 mesh C–X (specific surface area = 250 $m^2 g^{-1}$, Supelco, Belafonte, PA) was sieved to isolate granules in the size range of 180–212 μm, and then loaded into the device cavity *via* the loading ports under gentle suction pressure. Visual inspection was used to confirm when a single layer that filled the entire cavity had been achieved. Pre- and post-weighing of the device on an electronic balance indicated that ~750 μg of C–X was loaded. Fig. 3C shows the packaged and mounted device.

Performance testing

Test atmospheres of toluene vapor were generated dynamically by passing N_2 through a fritted bubbler containing the liquid solvent and then diluting in a metered flow of dry air. A portion of the flow was diverted every 5 min to a gas sampling loop mounted on a bench scale GC equipped with a flame ionization detector (FID) (Model 6890a, Agilent, Wilmington, DE) for confirmation of the toluene concentration. The FID was calibrated by auto-sampler syringe injections of liquid standards of toluene in CS_2. Injected masses ranged from 0.4 ng to 2.2 μg and the plot of peak area *vs.* mass injected (*i.e.*, calibration curve) was linear ($r^2 > 0.999$).

As part of a preliminary assessment of μPPI performance, the device was placed in the weighing chamber of a thermogravimetric analyzer (TGA) (Pyris 1, Perkin Elmer, Waltham, MA) and exposed to toluene. The μPPI was suspended from the weighing pan by a fine wire, and the N_2 purge line normally used to maintain an inert atmosphere within the semi-enclosed chamber was modified to permit switching from N_2 to a test atmosphere of toluene in N_2. The mass of the μPPI was recorded as a function of time to monitor toluene uptake in triplicate.

To characterize the sampling rate and desorption/injection efficiency of the device more thoroughly, the PCB-mounted μPPI was placed inside a custom-made 25 mL environmental chamber (Fig. 3C) in the system shown schematically in Fig. 4. A flow divider at the inlet to the chamber distributed the incoming flow (0.1 L min^{-1}) evenly over the raised device-mounting pedestal, and a portion of the exhaust flow was directed to a 250 μL sample loop mounted on a 6-port valve. The loop was alternately filled and then purged/injected into the GC inlet port (using a separate N_2 tank) in order to verify the test-atmosphere concentration (Fig. 4A). Following collection of a sample by the μPPI, the loop was replaced with a C–X-packed focuser (described immediately below), the upstream end of which was connected to the Macor® connector on the outlet port of the μPPI *via* a deactivated fused-silica capillary (sealed within one of the chamber exit lines), and the downstream end of which was connected *via* the 6-port valve, to a mini-pump (N86KNDCB, KNF Neuberger, Trenton, NJ) (Fig. 4B). During thermal desorption/injection of the μPPI sample, the mini-pump drew N_2 through the device and then the focuser. The valve was then switched and the focuser was heated rapidly and a separate N_2 tank was used to backflush the toluene desorbed from the focuser to the GC column (Fig. 4C). The mass of toluene injected was determined from the FID peak area by comparison with the calibration curve, previously generated for this experiment. Replacement of the focuser with the sample loop and collection of an additional sample allowed the chamber concentration to be checked post-exposure for residual toluene.

The focuser was a stainless steel tube (0.318 cm i.d.) packed with 5 mg of C–X (sieved to ~200 μm in diameter) held in place

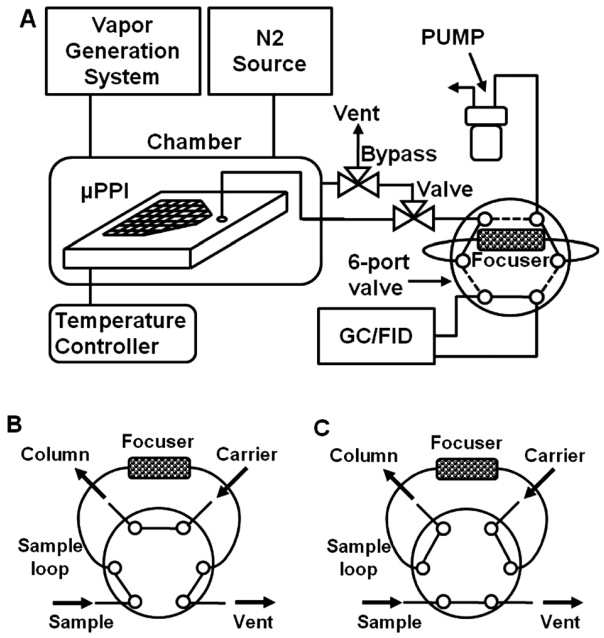

Fig. 4 (A) Schematic of the test setup used to characterize the sampling rate and the capture/transfer efficiency of the μPPI during thermal desorption. (B) The vapor sample is transferred from the μPPI to the focuser. (C) When the valve is switched, the sample in the focuser is thermally injected onto the column.

with a wire mesh and silanized glass wool. It was pre-conditioned initially at 300 °C for 12 h under N_2. The focuser was wrapped with an insulated Cu heater wire and thermally desorbed at 300 °C for 10 min, which served to transfer the toluene to the GC and re-condition the adsorbent for subsequent samples. The capacity of the focuser was verified in a separate series of tests showing that the mass of toluene captured and transferred to the GC matched that expected to be within 1.5%.

The PCB-mounted μPPI was placed on the pedestal in the center of the exposure chamber, electrical and fluidic interconnections were established, and the chamber was sealed and then purged with N_2. The system was programmed for repeated heating and cooling tests using LabView. The μPPI was pre-conditioned at 300 °C for 4 h. A constant concentration of 1 ppm of toluene vapor was passed through the chamber continuously and the μPPI was allowed to collect samples for discrete periods of 5, 10, 15, 20, 30, 40, 50, or 60 min. This concentration would be considered relatively low for industrial working environments and relatively high for typical office or residential environments.[37,38] We found it a convenient concentration level to use for this study because stable test atmospheres could be generated easily and the sampling times required to accumulate quantities of toluene above the detection limit of the FID were not excessively long. Tests were run in triplicate for each time period. Following each exposure, the chamber was purged for 3 min with 0.11 L min^{-1} of N_2 to remove any residual vapor. Then, the flow of N_2 through the chamber was stopped and the μPPI was rapidly self-heated to ~300 °C for 3 min to desorb the captured toluene. Prior to heating, a Tedlar bag filled with N_2 was connected to the chamber in order to provide make-up gas. The mini-pump was activated to draw the desorbed toluene through the device outlet port and the focuser for 6 min at a flow rate ranging from 10 to 50 mL min^{-1} (note: 50 mL min^{-1} was the default flow rate used for all experiments except those designed to examine the effect of varying flow rate on capture/injection efficiency). The 6-port valve was then actuated and the focuser was heated under a flow of N_2 at 1.8 mL min^{-1} to inject the captured vapor sample into the capillary column for elution and detection by the FID.

Results and discussions

Thermal response

To assess the thermal characteristics of the μPPI, the adsorbent loaded device was cycled between the ambient temperature and the target desorption temperature (300 °C) by repeatedly applying a constant bias of 12.5 V to the heater for 10 s and allowing it to cool for 190 s with air flowing through the device. For the 140 Ω baseline resistance of the meander line heater, this corresponds to an average of 1.1 W of dissipated power. Fig. S5 (ESI†) shows a series of temperature response profiles indicating that the floor of the cavity reaches 250 °C within 0.23 s and 300 °C within 3 s. The thermal cycling was continued for 100 hours, corresponding to ~2000 cycles, during which the time to reach the maximum temperature varied by <10% and the minimum and maximum temperatures varied by <3%. The power dissipation, thermal response, repeatability, and robustness exhibited by the device are all quite satisfactory.

Gravimetric estimation of sampling rate

Preliminary tests of the sampling rate performed with the TGA apparatus entailed continuous exposure to ~1.2 ppm of toluene for 60 min while monitoring the mass uptake. Eqn (1) was used to estimate S. Following a few minutes of induction, the mass uptake increased roughly linearly with time up to 24 min and then tapered off significantly. Unfortunately, fluctuations in the TGA output signal, which are attributable to flow-induced vibrations of the wire-suspended device, were significant. Applying a 120-pt running average to smooth the data,[39] followed by linear regression ($r^2 = 0.967$) yielded a value of $S = 9.8 \pm 0.49$ mL min^{-1} from the slope of the line. This is 5% higher than the aforementioned theoretical value of 9.3 mL min^{-1}. The total mass uptake for the linear portion of the curve was 0.86 μg, which is 45% of the total capacity of 2.1 μg. Given the mass resolution limitations of the TGA, the precision with which the slope and linear range can be estimated is limited. However, these results provide confirmation of expectations for a linear mass uptake period followed by a reduction in that rate as the fraction of occupied adsorption sites becomes large, in this case ~45% of the total predicted on the basis of the measured W_e value.

Chamber tests of sampling rate and desorption/injection efficiency

Subsequent tests, performed in the exposure chamber, afforded more accurate and precise estimates of S. Fig. 5 shows a plot of injected mass *versus* sampling time from 5 to 60 min. The relative standard deviation was ≤5% in all cases. Analysis of the residual toluene in the chamber headspace following each desorption led to values ranging from 3–7% of the amount initially injected,

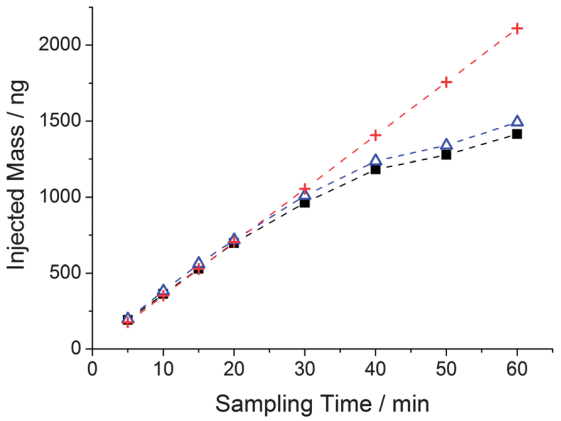

Fig. 5 Plots of the mass of toluene captured and thermally desorbed (injected) by the μPPI as a function of sampling time for a 1 ppm challenge concentration and a desorption (suction) flow rate of 50 mL min^{-1}. The red line (+symbol) reflects the expected mass uptake assuming the designed sampling rate of 9.3 mL min^{-1}. The black curve (filled squares) shows the experimental data obtained from the initial desorption of each sample. The blue curve (open triangles) shows the experimental data after addition of the residual mass of toluene that was not captured during the initial desorption. The reduction in the rate of mass uptake beyond 30 minutes reflects the decline in the sampling rate that occurs as the number of available surface sites on the adsorbent decreases.

which means that the capture/injection efficiency ranged from 93–97%. There was no apparent trend in transfer efficiency with sampled mass. These results indicate that the sampling/desorption performance of the μPPI is reproducible not only within a given sampling time but also over the entire series of experiments.

The mass uptake rate is constant up to ~30 min, after which it declines, in rough agreement with the results of the TGA experiments. A value of $S = 9.1$ mL min^{-1} was obtained from the slope of the linear region ($r^2 > 0.999$) of the curve after correcting for the residual mass of toluene not transferred during the initial desorption. This is only 2% lower than the theoretical prediction, and corresponds to a mass uptake rate of 34 ng min^{-1} at this concentration. The linear dynamic range of the mass uptake (*i.e.*, up to 30 min) was 1.01 μg, which corresponds to 48% of the total mass expected on the basis of W_e and indicates that above this level of adsorbent loading the assumption of efficient trapping by the adsorbent no longer holds. However, thermal desorption of the captured sample regenerates the device for subsequent use with no apparent degradation in performance. Beyond 30 min, the device continues to sample, but at a lower rate, which is expected to continue to decrease as the adsorption sites on the C–X become completely filled. At $t = 60$ min, the mass uptake was 1.5 μg, which is 71% of the total (2.1 μg) expected on the basis of the measured equilibrium adsorption capacity, W_e, assuming the designed sampling rate of 9.3 mL min^{-1}.

The capture/injection efficiency during thermal desorption was then examined as a function of the suction flow rate. For each of these tests, the device was exposed to 1 ppm of toluene for 15 min, leading to an expected mass uptake of 525 ng. The device was then heated while drawing flow from the downstream mini-pump at different flow rates. Results, plotted in Fig. 6, show that the capture efficiency decreases at a modest rate on going from 53 to 20 mL min^{-1} and at an apparently higher rate below 20 mL min^{-1}. The high efficiency observed at 52 mL min^{-1} (*i.e.*, 93%) is consistent with the results reported above and with predictions from CFD analysis.

To further explore this, a two-dimensional analytical model was developed (see Fig. S6 in the ESI†) for the capture/injection efficiency of the μPPI. The 2D model derives a mathematical formulation for the ratio of the sampled mass to the mass captured (and transferred to the focuser for GC analysis) during thermal desorption as a function of the suction flow rate. As shown by the dashed line in Fig. 6, the agreement of the model with the experimental results is reasonably good, particularly at the extremes of the range tested; the experimental value of 93% efficiency at the highest flow rate of 52 mL min^{-1} is only 7% lower than predicted by the model. Notably, a flow rate >10 mL min^{-1} is required to capture >50% of the desorbed vapor sample, hence the need for a focuser (or split-flow adaptor) to interface with a GC (micro)column.

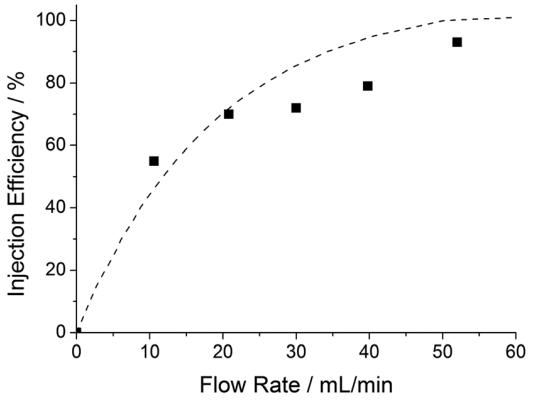

Fig. 6 Modeled (dashed line) and experimental (filled squares) values of capture/transfer (injection) efficiency *versus* suction flow rate for the μPPI.

Conclusions

This is the first report of a microfabricated passive VOC sampler. The μPPI also has an integrated resistive heater that permits *in situ* thermal desorption of captured vapor samples. The results presented demonstrate that the μPPI can capture VOCs from the air at low concentrations with zero power dissipation (*i.e.*, without active pumping) at a known and predictable rate. Efficient thermal desorption using the integrated heater and near-quantitative transfer of discrete samples to downstream components (with pumping) have also been documented.

The sampling rate of 9.1 mL min^{-1} observed for the test vapor, toluene, is remarkably high given the size of the device; similar rates would be expected from numerous other vapors with comparable diffusion coefficients in air, independent of the VOC concentration. Thus, sufficient mass can be collected within a few minutes from environments containing low- or sub-ppm concentrations to permit detection by any of a number of downstream microsensors (following focused injection and, possibly, chromatographic separation). The time span over which a given sampling rate can be maintained is a function of the vapor concentration and its affinity for the adsorbent material packed in the device. For 1 ppm of toluene and the graphitized carbon adsorbent, Carbopack X, used in the μPPI, we have shown that sampling is maintained at a constant rate for 30 minutes prior to having to thermally desorb the sample and regenerate the adsorbent surface. Repeated sampling/desorption cycles are possible, however, without any apparent effect on performance, which is a testament to the robust device design. These features augur well for the use of the μPPI in field-deployable μGC systems for personal exposure monitoring to assess the health impacts of VOCs.

The concept and designed functions of the μPPI have been validated analytically and experimentally using toluene as the test vapor. The experimental sampling rate is in excellent agreement with theory based on Fickian diffusion, and the heating power dissipation and capture efficiency of thermally desorbed samples are also in close agreement with the values predicted by the heat transfer and fluid dynamic models used to guide the device design and operating parameters.

Ongoing work is focused on characterizing the performance of the μPPI with other VOCs and VOC mixtures under conditions of varying concentrations to show its general utility. Integration with a micro-scale focuser, separation column and sensor-array detector to create low-power μGC systems is also planned.

Acknowledgements

The authors would like to thank Katharine Beach for assistance with device fabrication and Professor Kensall D. Wise and Rebecca Veeneman for early help with device design. This work was supported through the Michigan Center for Wireless Integrated Microsystems by the Engineering Research Centers Program of the National Science Foundation under Award Number ERC-9986866 and by a gift from Agilent Technologies. Devices described in this paper were fabricated in the Lurie Nanofabrication Facility, a member of the National Nanotechnology Infrastructure Network, which is supported by the National Science Foundation.

References

1 C.-J. Lu, W. H. Steinecker, W.-C. Tian, M. Agah, J. A. Potkay, M. C. Oborny, J. M. Nichols, H. K. L. Chan, J. Driscoll, R. D. Sacks, S. W. Pang, K. D. Wise and E. T. Zellers, *Lab Chip*, 2005, **5**, 1123–1131.
2 S. Zampolli, I. Elmi, F. Mancarella, P. Betti, E. Dalcanale, G. C. Cardinali and M. Severi, *Sens. Actuators, B*, 2009, **141**, 322–328.
3 P. R. Lewis, R. P. Manginell, D. R. Adkins, R. J. Kottenstette, D. R. Wheeler, S. S. Sokolowski, D. E. Trudell, J. E. Byrnes, M. Okandan, J. M. Bauer, R. G. Manley and G. C. Frye-Mason, *IEEE Sens. J.*, 2006, **6**, 784–795.
4 E. T. Zellers, G. Serrano, H. Chang and L. K. Amos, *Technical Digest Transducers' 11*, Beijing, China, June 5–9, 2011, pp. 2082–2085.
5 H. Kim, W. H. Steinecker, S. Reidy, G. R. Lambertus, A. A. Astle, K. Najafi, E. T. Zellers, L. P. Bernal, P. D. Washabaugh and K. D. Wise, *Technical Digest Transducers' 07*, Lyon, France, June 10–15, 2007, pp. 1505–1508.
6 S. K. Kim, H. Chang and E. T. Zellers, *Anal. Chem.*, 2011, **83**, 7198–7206.
7 I. Voiculescu, R. A. McGill, M. E. Zaghloul, D. Mott, J. Stepnowski, S. Stepnowski, H. Summers, V. Nguyen, S. Ross, K. Walsh and M. Martin, *IEEE Sens. J.*, 2006, **6**, 1094–1104.
8 R. A. Veeneman, PhD thesis, The University of Michigan, 2009.
9 B. Afeeli, D. Cho, M. Ashraf-Khorassani, L. T. Taylor and M. Agah, *Sens. Actuators, B*, 2008, **133**, 24–32.
10 W. C. Tian, S. W. Pang, C.-J. Lu and E. T. Zellers, *J. Microelectromech. Syst.*, 2003, **12**, 264–272.
11 W. C. Tian, H. K. L. Chan, C.-J. Lu, S. W. Pang and E. T. Zellers, *J. Microelectromech. Syst.*, 2005, **14**, 498–507.
12 I. Gracia, P. Ivanov, F. Blanco, N. Sabate, X. Vilanova, X. Correig, L. Fonseca, E. Figueras, J. Santander and C. Cane, *Sens. Actuators, B*, 2008, **132**, 149–154.
13 M. Martin, M. Crain, K. Walsh, R. A. McGill, E. Houser, J. Stepnowski, S. Stepnowski, H.-D. Wu and S. Ross, *Sens. Actuators, B*, 2007, **126**, 447–454.
14 R. P. Manginell, D. R. Adkins, M. W. Moorman, R. Hadizadeh, D. Copic, D. A. Porter, J. M. Anderson, V. M. Hietala, J. R. Bryan, D. R. Wheeler, K. B. Pfeifer and A. Rumpf, *J. Microelectromech. Syst.*, 2008, **17**, 1396–1407.
15 E. H. M. Camara, P. Breuil, D. Briand, L. Guillot, C. Pijolat and N. F. de Rooij, *Sens. Actuators, B*, 2010, **148**, 610–619.
16 J. Liu, N. K. Gupta, X. Fan, K. D. Wise and Y. B. Gianchandani, *Technical Digest Transducers 11*, Beijing, China, June 5–9, 2011, pp. 803–806.
17 http://www.schwarzer.com/pdf/SP_PUMPS_DataSheet_ClassFZ_Type135FZ.pdf.
18 http://www.knf.com/pdfs/nmp05_09_015.pdf.
19 http://divapps.parker.com/divapps/pnd/downloads/upd/CTS%20pump%20data%20sheet.pdf.
20 M. Agah, J. A. Potkay, G. Lambertus, R. Sacks and K. D. Wise, *J. Microelectromech. Syst.*, 2005, **14**, 1039–1050.
21 E. T. Zellers, S. Reidy, R. A. Veeneman, R. Gordenker, W. H. Steinecker, G. R. Lambertus, H. Kim, J. A. Potkay, M. P. Rowe, Z. Qiongyan, C. Avery, H. K. L. Sacks, K. Najafi and K. D. Wise, in *Technical Digest Trandsucers'07*, Lyon, France, June 10–15, 2007, pp. 1491–1496.
22 E. D. Palmes and A. F. Gunnison, *AIHAJ*, 1973, **34**, 78–81.
23 J. Namiesnik, B. Zabiegala, A. Kot-Wasik, M. Partyka and A. Wasik, *Anal. Bioanal. Chem.*, 2005, **381**, 279–301.
24 M. J. Boss and D. W. Day, *Air Sampling and Industrial Hygiene Engineering*, CRC Press, Boca Raton, FL, 2000.
25 B. A. Plog and P. J. Quinlan, *Fundamentals of Industrial Hygiene*, NSC Press, Itasca, IL, 5th edn, 2002.
26 http://www.skcinc.com/instructions/1667.pdf.
27 C.-W. Chung, M. T. Morandi, T. H. Stock and M. Afshar, *Environ. Sci. Technol.*, 1999, **30**, 3666–3671.
28 J. Gonzalez and S. P. Levine, *AIHAJ*, 1986, **47**, 339–346.
29 J. Gonzalez and S. P. Levine, *AIHAJ*, 1987, **48**, 739–744.
30 G. O. Nelson, *Gas Mixtures: Preparation and Control*, CRC Press, Boca Raton, FL, 1992.
31 A. Wheeler and A. J. Robell, *J. Catal.*, 1969, **13**, 299–305.
32 E. V. Kring and W. J. Lautenberger, *Du-pont US Pat.*, 4235097, 25 November 1980.
33 C. J. Lu and E. T. Zellers, *Analyst*, 2002, **127**, 1061–1068.
34 C. J. Lu and E. T. Zellers, *Anal. Chem.*, 2001, **73**, 3449–3457.
35 http://www.sigmaaldrich.com/analytical-chromatography/air-monitoring/learning-center/adsorbent-selection.html.
36 F. M. White, *Fluid Mechanics*, McGraw-Hill, New York, NY, 10th edn, 2010.
37 American Conference of Governmental Industrial Hygienists, *Threshold Limit Values for Chemical Substances and Physical Agents and Biological Exposure Indices*, ACGIH, Cincinnati, OH, 2011.
38 C.-Y. Peng and S. Batterman, *J. Environ. Monit.*, 2000, **2**, 313–324.
39 S. Ross, *Statistics for Engineers and Scientists*, Elsevier Academic Press, Waltham, MA, 4th edn, 2009.

